



Contents lists available at ScienceDirect

Journal of Biomechanics

journal homepage: www.elsevier.com/locate/jbiomech
www.JBiomech.com

Chiral behavior in rat tail tendon fascicles

Kimberly A. Buchanan^{a,b}, Roderic S. Lakes^{c,d}, Ray Vanderby Jr.^{a,b,c,*}

^a Department of Biomedical Engineering, University of Wisconsin-Madison, Madison, WI 53706, USA

^b Department of Orthopedics and Rehabilitation, University of Wisconsin-Madison, Madison, WI 53705, USA

^c Materials Science Program, University of Wisconsin-Madison, Madison, WI 53706, USA

^d Department of Engineering Physics, University of Wisconsin-Madison, Madison, WI 53706, USA

ARTICLE INFO

Article history:

Accepted 25 September 2017

Available online xxx

Keywords:

Tendon
Fascicle
Mechanics
Chirality
Cosserat elasticity

ABSTRACT

Ex vivo tendon mechanical behavior has been well described under rotationally constrained uniaxial tensile testing. During standard loading of rat tail tendon (RTT) fascicles, apparent axial twist has been observed. To quantify this behavior, we designed a custom testing setup, utilizing magnetic suspension, to allow unconstrained axial rotation during tensile loading. We characterized the rotational behavior of single and paired RTT fascicles under cyclic loading. We also measured stress relaxation across loading cycles as well as “rotational relaxation”. Single fascicle nonlinear stretch-twist coupling is well described by the asymptotic function $\Delta\theta = A(1 - e^{-B\epsilon})$ in which fascicles rotated a mean $\pm 51.1^\circ$ within about 1% applied axial strain. On average, paired fascicles rotated just over 10° less. Specimen cross-sectional diameter had a noticeable effect on the measured mechanical properties, particularly effective elastic modulus. Such stretch-twist coupling and size dependence cannot be understood via classical elasticity but is predicted by Cosserat (micropolar) elasticity. The current study demonstrates RTT fascicles are chiral based on observed axial load-induced twist. Additionally, our findings support existing research that suggests a helical fascicle structure. Potential consequences of helical substructures, mechanical and biological, merit further investigation.

© 2017 Published by Elsevier Ltd.

1. Introduction

Tendon absorbs and transfers load between muscle and bone, and its mechanical properties are dependent on its hierarchical structure. The largest substructure of tendon is the fascicle, which is composed of fibers made up of fibrils. A mature fibril is very long and consists of self-assembled collagen molecules (Kadler et al., 1996; Kastelic et al., 1978; Provenzano and Vanderby, 2006; Screen et al., 2004a). This hierarchical organization has been shown to attenuate strain in the substructures, which experience smaller strains than whole tendon (Puxkandl et al., 2002; Screen et al., 2004b; Thorpe et al., 2012). For example, fascicles only stretch 55–90% of the 4–6% in vivo whole tendon strain (Gardiner et al., 2001; Kongsgaard et al., 2011; Lochner et al., 1980; Thorpe et al., 2012). Contributing mechanisms include the sliding that occurs between adjacent fascicles (Screen et al., 2004a, 2004b; Thorpe et al., 2012).

Ex vivo mechanical testing of tendon tissue is typically performed with rotationally constrained uniaxial tensile loading to

provide a reproducible estimate of the physiological system. During tensile testing of rat tail tendon (RTT) fascicles, researchers observed rotational movement of visual strain markers (Cheng and Screen, 2007; Screen, 2008). We noted similar axial twist when mechanically stretching RTT fascicles. The presence of load-induced twist would imply fascicles are chiral, meaning they lack symmetry about their rotational axis. A ubiquitous and biologically relevant example is the helix. Helical structures have been identified at multiple hierarchical levels within tendon. The collagen I molecule is a right-handed triple helix made from three left-handed polypeptide helices. Collagen molecules self-assemble into right-handed, super-twisted microfibrils, which interdigitate with neighboring microfibrils. These units, in turn, self-assemble into larger hierarchical structures (Duenwald et al., 2009; Franchi et al., 2010; Orgel et al., 2006; Ramachandran and Kartha, 1955; Silver et al., 2003). Fiber and fascicle level helical windings have been visualized as well (Jozsa et al., 1991; Kalson et al., 2012; Kannus, 2000; Khodabakhshi et al., 2013; Thorpe et al., 2013; Vidal, 2003). Additionally, computer modeling supports the theory of higher level helices (Reese et al., 2010; Zhao et al., 2016). Helical structure could contribute to stress attenuation while increasing strain, thus leading to nonlinear load uptake (Wang et al., 2016).

* Corresponding author at: Department of Orthopedics and Rehabilitation, University of Wisconsin-Madison, 1111 Highland Ave., Room 5059, Madison, WI 53705, USA.

E-mail address: vanderby@ortho.wisc.edu (R. Vanderby Jr.).

Notation

L_0	initial length	$\Delta\theta$	rotation
ΔL	displacement	+	clockwise
ε	axial strain	-	counterclockwise
γ	shear strain	r_{avg}	average radius
σ	stress	A, B	coefficients

Tendon has been extensively characterized as a viscoelastic, nonlinear, and anisotropic material at an apparent tissue level (Kondratko et al., 2012; Lake et al., 2009; Lynch et al., 2003; Screen, 2008; Woo et al., 1993). Existing classically elastic or viscoelastic models are not capable of modeling stretch-twist coupling behavior. An alternative that permits axial strain-rotation coupling is the Cosserat, or micropolar, theory of elasticity. Cosserat theory allows for the microrotation of points in addition to the translation afforded by classical elasticity. Instead of only 2 elastic constants, Cosserat elasticity uses 6 constants for isotropic solids and 9 for directionally isotropic chiral solids that exhibit stretch-twist coupling. A notable consequence is the presence of a size effect, or size dependence, which is not predicted in classical elasticity (Lakes, 1995; Lakes, 2001; Lakes and Benedict, 1982). Cosserat mechanics has already been applied to descriptions of biological materials such as bone and actin filaments (Park and Lakes, 1986; Yamaoka and Adachi, 2010).

To our knowledge, unconstrained rotation of tendon tissue has not been quantified experimentally. Similarly, Cosserat mechanics has not been considered for tendon behavior. The current study characterizes the rotational behavior of RTT fascicle using Cosserat mechanics as a guide. Individual fascicles and naturally occurring pairs of fascicles are examined for a hierarchical comparison. We hypothesize RTT fascicles will exhibit stretch-twist coupling and size effects, as predicted by Cosserat elasticity; we expect the effects will be nonlinear in view of known nonlinearity of axial stress-strain curves. Additionally, we hypothesize that cyclic stress relaxation will occur in the context of axially induced rotations. Our findings may have implications for hierarchical tendon descriptions and mechanical models. Chiral behavior would also prompt investigation into the effects stretch-twist coupling have on cell signaling and mechanotransduction.

2. Methods**2.1. Specimen preparation**

Fifteen (15) Wistar rats, age 2–3 months and weight 225–325 g, were humanely euthanized as approved by the University of Wisconsin Institutional Animal Use and Care Committee. The tails were kept frozen at $-10\text{ }^{\circ}\text{C}$ until use. Once thawed, the skin was removed to expose the left dorsal tendon. Under a dissecting microscope, fascia was carefully cut to reveal fascicles. Intact pairs of fascicles were isolated and are hereinafter referred to as paired fascicles in which 1 specimen consists of 2 fascicles with intact intra-fascicular tissue. Further dissection provided single fascicle specimens. All specimens were at least 50 mm long from the proximal end. Twenty (20) single fascicles and ten (10) paired fascicles, a total of 30 specimens, were dissected and immediately tested. An average of 2, and maximum of 3, specimens were collected from a single tendon. Hydration was maintained throughout with phosphate-buffered saline (PBS).

2.2. Mechanical testing

A custom setup within a standard servo-hydraulic testing machine (MTS Bionix 858; Eden Prairie, Minnesota) was used for mechanical testing (Fig. 1). A specimen was placed into custom spring-loaded grips spaced 45.6 mm ($SD = 1.3$) apart within a PBS bath. The lower grip was fixed to the MTS platform. The upper grip connected to a vane and a ferromagnetic rod via a 0.85-mm diameter nylon line. The rod was suspended 12.8 mm ($SD = 0.4$) from a 5 N capacity magnet attached to the actuator and a 222 N load cell. Magnetic suspension allowed frictionless rotation of the specimen and attached vane. The vane was aligned in the path of an optical LED micrometer (Keyence Corp LS-7030T; Osaka, Japan) that

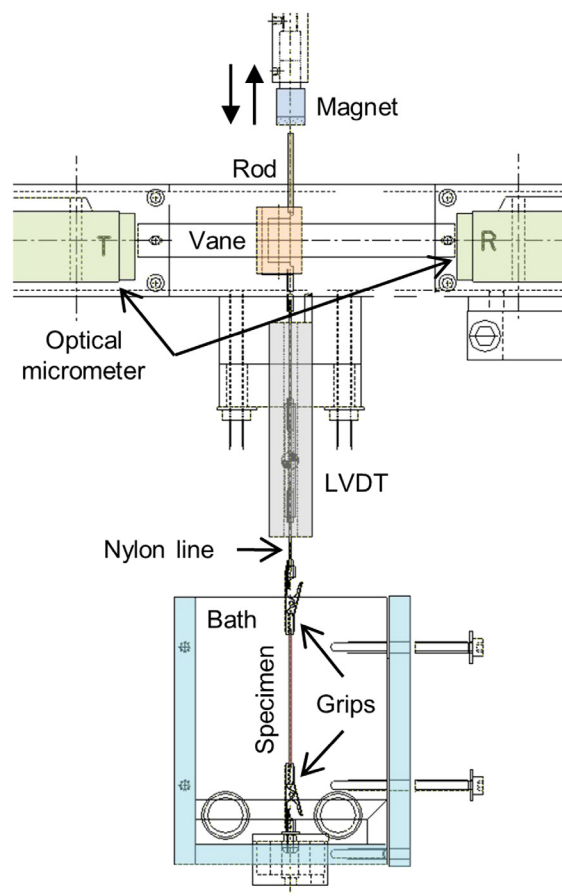


Fig. 1. Custom setup within a servo-hydraulic test machine for measuring unconstrained axial rotation of a tissue specimen during uniaxial tensile loading. A specimen was gripped and submerged in phosphate-buffered saline. Force on the specimen-vane-rod system changed as the actuator and magnet displaced. Specimen rotation was computed from optical micrometer data monitoring rotationally induced changes in the projected vane width. Specimen axial deformation was measured by a linear variable differential transformer (LVDT).

recorded the vane's projected width. When the displacement-controlled actuator lowered towards the rod, the magnet caused an increase in tensile force on the specimen. Due to the nonlinear magnetic field and the typical strain stiffening tissue behavior, the applied tensile force was nonlinear relative to magnet displacement (Fig. 2). Specimen deformation was measured using a linear variable differential transformer (LVDT) (Measurement Specialties Inc DC-EC 250; Hampton, Virginia) with its inner core positioned over the lowest portion of the nylon line. At approximately twice the diameter of the specimen, the nylon line's torsional rigidity was approximately 16 times that of the specimen. Therefore, vane rotation was attributed to specimen rotation.

With the rod suspended from the magnet, the magnetic force on the specimen served as a preload of 0.11 N (SD = 0.03), which corresponded to a preload strain of 0.7% (SD = 0.8). The magnet was cyclically displaced between its starting position and a peak displacement of 6.3 mm (SD = 0.2) downward toward the rod. The displacement-controlled protocol followed a cosine waveform consisting of 5 cycles at 0.5 cycle/min (Fig. 2). Data, including micrometer and LVDT voltages, were acquired at 10 Hz and output to a PC with Labtech Notebook software (Laboratory Technology Corp; Fort Collins, Colorado). Micrometer voltages were correlated to projected vane widths then vane angles via a sixth-order polynomial. LVDT voltage changes were proportional to axial displacement.

2.3. Parameter calculations

Assuming an elliptic geometry, specimen cross-sectional area was calculated based on major and minor diameters measured prior to testing. Each specimen was vertically suspended perpendicular to the horizontal field of the optical micrometer and axially rotated until the largest, midsection diameter (major diameter) was visualized and measured. The specimen was then rotated 90° to obtain the minor, midsection diameter measurement. Average diameter and radius were used for size effect analysis and shear strain calculation, respectively. Specimen axial strain (ϵ) was determined by dividing the LVDT-measured displacement (ΔL) by the preloaded, grip-to-grip specimen length (L_0): $\epsilon = \Delta L/L_0$. The absolute change in vane angle was termed axial rotation with rotation direction noted by the sign: positive (+) = clockwise (CW) and negative (–) = counterclockwise (CCW). Specimen shear strain (γ) was calculated as the measured rotation ($\Delta\theta$) multiplied by the average radius (r_{avg}) and divided by the initial, preloaded length: $\gamma = \Delta\theta r_{avg}/L_0$.

The loading portion of cycle 1 was isolated to evaluate the stretch-twist relationship. The asymptotic function

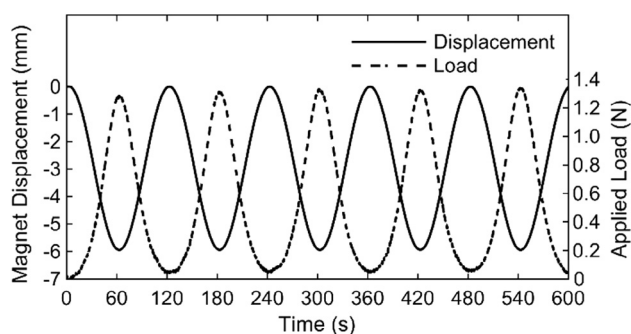


Fig. 2. Testing protocol was a displacement-controlled cosine waveform (solid line). The nonlinear magnetic field resulted in the representative, nonlinear loading waveform (interrupted line). The actuator and magnet were lowered 6.3 mm (SD = 0.2) toward the ferromagnetic rod and returned for 5 complete cycles at 0.5 cycle/min. At least 1 N of load was applied to the specimen.

$\Delta\theta = A(1 - e^{-B\epsilon})$ was used to quantify the behavior between axial strain and rotation. Stress-strain ratios (σ/ϵ) and shear strain to axial strain ratios (γ/ϵ) were compared to average diameters for possible size effects. Shear-to-axial strain ratio quantifies the coupling between axial stretch and twist rotation and is a parameter utilized in Cosserat elastic descriptions. Ratios were calculated at the time point when cycle 1 peak rotation occurred. Peak stress and peak rotation within each cycle were compared for potential specimen relaxation behavior. Peak stress and rotation were normalized by corresponding peak strain values. Normalized stress and rotation were then normalized to cycle 1 for comparing specimens.

2.4. Statistical analysis

Mean and standard deviation (SD) were reported for all parameters. Stretch-twist curve fit coefficients and R^2 values were calculated. Linear regressions were performed on the size effect data. One-way ANOVAs with Tukey's post hoc tests were performed to compare single and paired fascicles, and cycles. Statistical significance was defined as $p < .05$.

2.5. Scanning electron microscopy

Single and paired fascicles were imaged with scanning electron microscopy (SEM) to observe the underlying fibrillar structure. Immediately after dissection, specimens, about 10 mm long from the proximal end, were fixed in 2.5% glutaraldehyde in PBS for 8 h. Specimens were dehydrated in ascending ethanol concentrations up to 100% and critical point dried. Finally, specimens were sputter coated in palladium/gold and visualized using a high-resolution scanning electron microscope (Hitachi S-3200N; Tokyo, Japan).

3. Results

3.1. Stretch-twist coupling

For single fascicles, the loading portion of the first cycle revealed a non-linear relationship between applied axial strain and measured axial rotation (Fig. 3A). The fascicles rotated 51.1° on average (SD = 19.9), most of which occurred within the first 1% strain after preloading. Paired fascicles exhibited less rotation with a mean 39.7° (SD = 22.7), a non-significant trend ($p = 0.157$).

Rotation was observed in both CW and CCW directions. For the 20 single fascicles tested, 10 rotated CW and 10 CCW. Of the 10 paired fascicles, 6 rotated CW and 4 CCW. Having noted which single fascicles were originally paired, single fascicles did not consistently rotate in either the same or opposite direction as the counterpart in the pair.

The stretch-twist coupling was well described by the asymptotic function $\Delta\theta = A(1 - e^{-B\epsilon})$ (Fig. 3B). The mean calculated function coefficients $|A|$ and B were 49.7 (SD = 18.0) and 3.37 (SD = 1.17), respectively. The mean goodness-of-fit R^2 value was 0.993 (SD = 0.008).

3.2. Diameter size effect

Stress-strain ratio, or effective modulus, appeared to correlate to average fascicle diameter for single and paired fascicles (Fig. 4A). For single and paired fascicles, the linear regression R^2 values were 0.773 and 0.794, respectively. The mean average diameter for single fascicles was 474 μm (SD = 53) and for paired fascicles was 509 μm (SD = 81; $p = 0.175$). The mean stress-strain

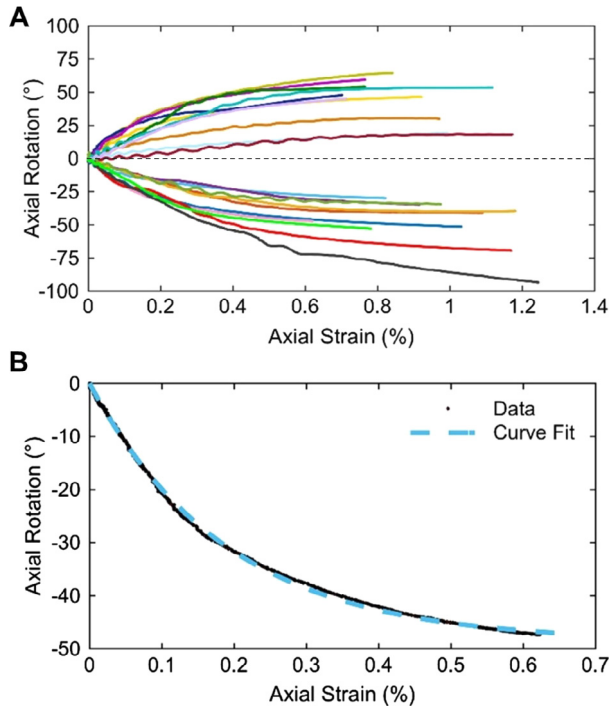


Fig. 3. Cycle 1 loading of single fascicles. (A) Applied percent fascicle strain and the measured degrees of rotation (+ = clockwise, - = counterclockwise) for each fascicle ($n = 20$). (B) Representative fascicle rotation-strain curve (black closed circle) with the asymptotic curve fit $\Delta\theta = A(1 - e^{-B\epsilon})$ (interrupted blue line; $A = -48.7$, $B = 5.27$, $R^2 = 0.999$). (For interpretation of the references to colour in this figure legend, the reader is referred to the web version of this article.)

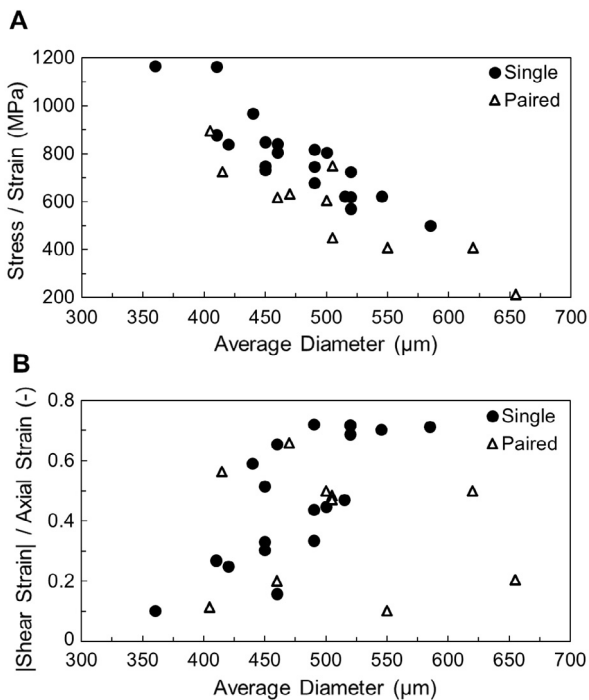


Fig. 4. Effect of average single fascicle diameter (closed circle; $n = 20$) and average paired fascicle diameter (open triangle; $n = 10$) on (A) stress-strain ratio ($R^2 = 0.773$ and 0.794 , respectively) and (B) shear strain to axial strain ratio ($R^2 = 0.576$ and 0.013 , respectively).

ratio for single and paired fascicles was 785 MPa ($SD = 173$) and 569 MPa ($SD = 201$), respectively ($p < .01$).

Shear strain to axial strain ratio, another representation of stretch-twist coupling, and average diameter did not correlate as

strongly (Fig. 4B). R-squared values for single and paired fascicles were 0.576 and 0.013 , respectively. The mean shear-to-axial strain ratio for single and paired fascicles was 0.470 ($SD = 0.208$) and 0.380 ($SD = 0.202$), respectively ($p = 0.270$).

3.3. Cyclic stress relaxation

Normalized peak stress and normalized peak rotation were calculated for each of the 5 cycles. Peak stresses and peak rotations were normalized by corresponding peak axial strains then normalized to cycle 1. Single fascicles exhibited a reduction in normalized peak stress with each subsequent cycle (Fig. 5A). Statistically significant differences were found between all cycle comparisons ($p = 0.003$ for cycle 4 v 5, $p < .0001$ for all others). Normalized peak stress progressively lowered between cycles for paired fascicles as well (Fig. 5B). Compared to cycle 1, there were significant reductions for cycles 3, 4, and 5 ($p = 0.004$, 0.002 , and 0.0003 , respectively).

Similarly, single and paired fascicles demonstrated smaller normalized peak rotations with each subsequent cycle. For single fascicles, cycles 2, 3, 4, and 5 were significantly less than cycle 1 (cycle 2: $p = 0.0001$, cycles 3–5: $p < .0001$) (Fig. 5C). Additionally, cycles 4 and 5 were significantly less than cycle 2 ($p = 0.003$ and $p < .0001$, respectively). Paired fascicles only had significantly smaller rotations with cycles 4 and 5 when compared to cycle 1 ($p = 0.016$ and $p = 0.004$, respectively) (Fig. 5D).

3.4. Scanning electron microscopy

Helical organization of the fibers could explain the observed fascicle rotation. Although the fibers were not obviously angled relative to the single fascicle (Fig. 6A), calculations indicate that fiber

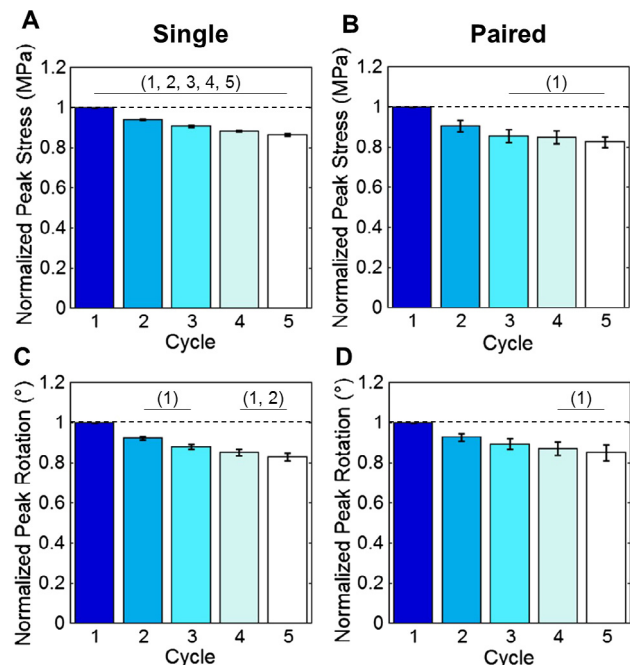


Fig. 5. Peak stress normalized by corresponding peak strain across 5 cycles and normalized to cycle 1: (A) for single fascicles ($n = 20$), all cycle comparisons were different ($p < .01$), and (B) for paired fascicles ($n = 10$), cycles 3–5 were reduced compared to cycle 1 ($p < .01$). Peak rotation normalized by corresponding peak strain across 5 cycles and normalized to cycle 1: (C) for single fascicles, cycles 2–5 were smaller than cycle 1 ($p < .001$) and cycles 4–5 were smaller than cycle 2 ($p < .01$), and (D) for paired fascicles, cycles 4–5 were smaller than cycle 1 ($p < .05$). Error bars represent standard error. (1) = significantly different from cycle 1, (2) = significantly different from cycle 2, and so on ($p < .05$).

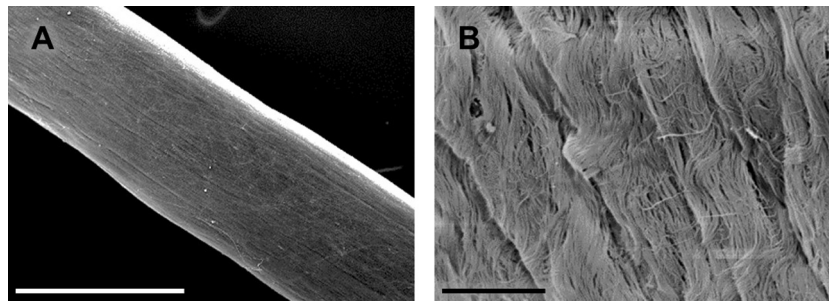


Fig. 6. Single fascicle surface imaged with scanning electron microscopy to visualize structural organization of (A) the fibers within a fascicle, which appeared relatively linear (bar = 500 μm), and (B) the fibrils within the fibers, which appeared to show right-handed helical winding of the fibrils (bar = 10 μm).

helical angles less than one degree would account for the measured axial rotations, given the fascicle length and radius. Upon closer examination, some images showed fibers being composed of right-handed helical fibrils (Fig. 6B). No discernable differences were noted between fascicles within a pair.

4. Discussion

Overall, this study supports our hypotheses that RTT fascicles exhibit nonlinear stretch-twist coupling and size effects, and that there is cyclic relaxation in terms of rotation. The custom-built testing setup allowed measurement of unconstrained axial rotation during uniaxial tensile loading. Single fascicles displayed nonlinear stretch-twist coupling that leveled off within about 1% strain after a notable mean $\pm 51.1^\circ$ of rotation. Paired fascicles rotated just over 10° less than single fascicles; however, the difference was statistically insignificant. Smaller rotations of paired fascicles might be explained by opposing handedness of the individual fascicles. Our fascicles did not all rotate in the same direction, which was also noted by Cheng and Screen (2007). We observed clockwise and counterclockwise rotations, and the distribution was approximately 50:50. Furthermore, pairs of fascicles were inconsistent in that both same and opposing rotation directions were seen within a given pair. Handedness may also be influenced by the mediolateral fascicle location within a tendon and by the tendon location within a rat tail, but those factors were not explored.

Based on the observed behavior, we conclude RTT fascicles act as chiral materials. As a result, current classically elastic models and viscoelastic models are insufficient to capture this behavior. Use of an alternative theory, Cosserat elasticity, accounts for the point rotations needed to predict stretch-twist coupling in chiral rods (Lakes, 1995; Lakes, 2001; Lakes and Benedict, 1982). It is worth noting that allowing fascicles to freely rotate did not have a strong effect on the mean effective modulus. The modulus of single fascicles, 785 ± 173 MPa, was comparable to moduli of just over 800 MPa determined during rotationally constrained tensile testing (LaCroix et al., 2013). Introducing chiral structures, which exhibit twist deformation, will reduce the elastic modulus and Poisson's ratio of a material. Chiral descriptions predict hydrostatic stress in the core, which may contribute to interstitial fluid flow and altered tractions at the intra-fascicular surfaces. Since this may affect local mechanotransduction, the chiral nature of fascicles should be borne in mind for cellular level probes of tendon mechanotransduction.

Size effects, which are not present in classically elastic solids, are seen in chiral Cosserat solids. The data revealed a strong and inverse average-diameter size effect on effective modulus. The effect, $\sigma/\varepsilon \propto 1/D$, extended into the larger paired fascicles. Elsewhere, modulus was found to be inversely dependent on the cross-sectional area of rotationally constrained RTT fascicles (Legerlotz et al., 2010). Overall, evidence of size dependence has

been shown, which supports the use of Cosserat elasticity to describe chiral fascicles.

In the present study, size had a weak linear effect on shear strain to axial strain ratio, a measure of stretch-twist coupling, for single fascicles. There was no linear correlation for paired fascicles. If the specimen radius was sufficiently large compared to the material characteristic length scale, and if the material contained chiral microstructures uniformly distributed over the volume, then an inverse relationship would be predicted for shear-to-axial strain ratio ($\gamma/\varepsilon \propto 1/D$) (Lakes and Benedict, 1982). Based on the SEM images, the latter structural requirement was not met in RTT fascicles. Therefore, the lack of an inverse size effect is not surprising. Nevertheless, fascicles exhibited large values of stretch-twist coupling at small strains: the ratio of shear-to-axial strain was comparable to that in 3D isotropic chiral lattices designed to exhibit such effects (Ha et al., 2016).

To examine how fascicles behaved across all 5 cycles, we analyzed cyclic relaxation. We observed that load imparted by the test system produced irrecoverable strain within a given cycle causing strain to creep with each cycle. Single and paired fascicles exhibited stress relaxation and its rotational equivalent: rotational relaxation. The amount of stress per unit strain and rotation per unit strain decreased with each cycle.

A structural explanation for the observed chirality was briefly probed for using SEM imaging. Some images showed right-handed helical winding of fibrils to form the fibers. Those who have looked more extensively have also identified helices at this fiber level (Franchi et al., 2010), although Kalson et al. (2015) notes a clear majority were left-handed helices in mouse tail tendon. Szczesny et al. (2015) calculated fibril trajectory to be angled $1.7 \pm 1^\circ$ relative to the RTT fascicle suggesting a non-planar organization. However, these helices would not account for the chirality witnessed at a higher hierarchical level. Images were inconclusive regarding a helical organization of fibers within a fascicle. Even so, the present experiment demonstrated substantial axial rotation during tensile loading of RTT fascicles, which supports the theory of helical organization at the fascicle level.

Integration of helical structures, especially at the fiber and fascicle levels, may be pertinent to future models and descriptions. Cosserat mechanics predicts stretched chiral rods to exhibit a non-uniform Poisson-type transverse deformation. As a result, possible non-uniform hydrostatic stress would lead to hydrostatic pressure changes within fascicles. This might contribute to various aspects of cellular behavior including cell homeostasis, cell signaling, and fluid transport. Further study of the mechanical and biological consequences of chiral behavior is warranted.

Conflict of interest statement

The authors have no conflicts of interest to disclose.

Acknowledgments

Support by the National Science Foundation (Award 1432937) is gratefully acknowledged. The authors also thank Ron McCabe for his technical assistance constructing the testing setup, and Heather Hartwig Stokes and Andrew Close for their assistance with data collection.

References

- Cheng, V.W.T., Screen, H.R.C., 2007. The micro-structural strain response of tendon. *J. Mater. Sci.* 42 (21), 8957–8965.
- Duenwald, S.E., Vanderby, R., Lakes, R.S., 2009. Viscoelastic relaxation and recovery of tendon. *Ann. Biomed. Eng.* 37 (6), 1131–1140.
- Franchi, M., De Pasquale, V., Martini, D., Quaranta, M., Macciocca, M., Dionisi, A., Ottani, V., 2010. Contribution of glycosaminoglycans to the microstructural integrity of fibrillar and fiber crimps in tendons and ligaments. *Sci. World J.* 10, 1932–1940.
- Gardiner, J.C., Weiss, J.A., Rosenberg, T.D., 2001. Strain in the human medial collateral ligament during valgus loading of the knee. *Clin. Orthop. Relat. Res.* 391, 266–274.
- Ha, C.S., Plesha, M.E., Lakes, R.S., 2016. Chiral three-dimensional isotropic lattices with negative Poisson's ratio. *Phys. Status Solidi (B)* 253 (7), 1243–1251.
- Jozsa, L., Kannus, P., Balint, J.B., Reffy, A., 1991. Three-dimensional ultrastructure of human tendons. *Acta Anat.* 142 (4), 306–312.
- Kadler, K.E., Holmes, D.F., Trotter, J.A., Chapman, J.A., 1996. Collagen fibril formation. *Biochem. J.* 316 (1), 1–11.
- Kalson, N.S., Lu, Y., Taylor, S.H., Starborg, T., Holmes, D.F., Kadler, K.E., 2015. A structure-based extracellular matrix expansion mechanism of fibrous tissue growth. *eLife* 4, e05958.
- Kalson, N.S., Malone, P.S.C., Bradley, R.S., Withers, P.J., Lees, V.C., 2012. Fibre bundles in the human extensor carpi ulnaris tendon are arranged in a spiral. *J. Hand Surg.* 37 (6), 550–554.
- Kannus, P., 2000. Structure of the tendon connective tissue. *Scand. J. Med. Sci. Sports* 10 (6), 312–320.
- Kastelic, J., Galeski, A., Baer, E., 1978. The multicomposite structure of tendon. *Connect. Tissue Res.* 6 (1), 11–23.
- Khodabakhshi, G., Walker, D., Scutt, A., Way, L., Cowie, R.M., Hose, D.R., 2013. Measuring three-dimensional strain distribution in tendon. *J. Microsc.* 249 (3), 195–205.
- Kondratko, J., Duenwald-Kuehl, S., Lakes, R., Vanderby, R., 2012. Mechanical compromise of partially lacerated flexor tendons. *J. Biomech. Eng.* 135 (1), 011001(1)–011001(8).
- Kongsgaard, M., Nielsen, C.H., Hegnsvad, S., Aagaard, P., Magnusson, S.P., 2011. Mechanical properties of the human Achilles tendon, in vivo. *Clin. Biomech.* 26 (7), 772–777.
- LaCroix, A.S., Duenwald-Kuehl, S.E., Brickson, S., Akins, T.L., Diffie, G., Aiken, J., Vanderby, R., Lakes, R.S., 2013. Effect of age and exercise on the viscoelastic properties of rat tail tendon. *Ann. Biomed. Eng.* 41 (6), 1120–1128.
- Lake, S.P., Miller, K.S., Elliott, D.M., Soslowsky, L.J., 2009. Effect of fiber distribution and realignment on the nonlinear and inhomogeneous mechanical properties of human supraspinatus tendon under longitudinal tensile loading. *J. Orthop. Res.* 27 (12), 1596–1602.
- Lakes, R.S., 1995. Experimental methods for study of Cosserat elastic solids and other generalized elastic continua. In: Mühlhaus, H.B. (Ed.), *Continuum models for materials with microstructure*. Wiley, New York, pp. 1–22.
- Lakes, R.S., 2001. Elastic and viscoelastic behavior of chiral materials. *Int. J. Mech. Sci.* 43 (7), 1579–1589.
- Lakes, R.S., Benedict, R.L., 1982. Noncentrosymmetry in micropolar elasticity. *Int. J. Eng. Sci.* 20 (10), 1161–1167.
- Legerlotz, K., Riley, G.P., Screen, H.R.C., 2010. Specimen dimensions influence the measurement of material properties in tendon fascicles. *J. Biomech.* 43 (12), 2274–2280.
- Lochner, F.K., Milne, D.W., Mills, E.J., Groom, J.J., 1980. In vivo and in vitro measurement of tendon strain in the horse. *Am. J. Vet. Res.* 41 (12), 1929–1937.
- Lynch, H.A., Johannessen, W., Wu, J.P., Jawa, A., Elliott, D.M., 2003. Effect of fiber orientation and strain rate on the nonlinear uniaxial tensile material properties of tendon. *J. Biomech. Eng.* 125 (5), 726–731.
- Orgel, J.P.R.O., Irving, T.C., Miller, A., Wess, T.J., 2006. Microfibrillar structure of type I collagen in situ. *Proc. Nat. Acad. Sci. USA.* 103 (24), 9001–9005.
- Park, H.C., Lakes, R.S., 1986. Cosserat micromechanics of human bone: strain redistribution by a hydration-sensitive constituent. *J. Biomech.* 19 (5), 385–397.
- Provenzano, P.P., Vanderby, R., 2006. Collagen fibril morphology and organization: Implications for force transmission in ligament and tendon. *Matrix Biol.* 25 (2), 71–84.
- Puxkandl, R., Zizak, I., Paris, O., Keckes, J., Tesch, W., Bernstorff, S., Fratzl, P., 2002. Viscoelastic properties of collagen: synchrotron radiation investigations and structural model. *Philos. Trans. Royal Soc. B: Biol. Sci.* 357 (1418), 191–197.
- Ramachandran, G.N., Kartha, G., 1955. Structure of collagen. *Nature* 176 (4482), 593–595.
- Reese, S.P., Maas, S.A., Weiss, J.A., 2010. Micromechanical models of helical superstructures in ligament and tendon fibers predict large Poisson's ratios. *J. Biomech.* 43 (7), 1394–1400.
- Screen, H.R.C., 2008. Investigating load relaxation mechanics in tendon. *J. Mech. Behav. Biomed. Mater.* 1 (1), 51–58.
- Screen, H.R.C., Bader, D.L., Lee, D.A., Shelton, J.C., 2004a. Local strain measurement within tendon. *Strain* 40 (4), 157–163.
- Screen, H.R.C., Lee, D.A., Bader, D.L., Shelton, J.C., 2004b. An investigation into the effects of the hierarchical structure of tendon fascicles on micromechanical properties. *Proc. Inst. Mech. Eng. [H]* 218 (2), 109–119.
- Silver, F.H., Freeman, J.W., Seehra, G.P., 2003. Collagen self-assembly and the development of tendon mechanical properties. *J. Biomech.* 36 (10), 1529–1553.
- Szczesny, S.E., Caplan, J.L., Pedersen, P., Elliott, D.M., 2015. Quantification of interfibrillar shear stress in aligned soft collagenous tissues via notch tension testing. *Sci. Rep.* 5, 14649.
- Thorpe, C.T., Klemm, C., Riley, G.P., Birch, H.L., Clegg, P.D., Screen, H.R.C., 2013. Helical sub-structures in energy-storing tendons provide a possible mechanism for efficient energy storage and return. *Acta Biomater.* 9 (8), 7948–7956.
- Thorpe, C., Udeze, C.P., Birch, H.L., Clegg, P.D., Screen, H.R.C., 2012. Specialization of tendon mechanical properties results from interfascicular differences. *J. Royal Soc. Interface* 9 (76), 3108–3117.
- Vidal, B.C., 2003. Image analysis of tendon helical superstructure using interference and polarized light microscopy. *Micron* 34 (8), 423–432.
- Wang, L., Cui, Y., Qin, Q., Wang, H., Wang, J., 2016. Helical fiber pull-out in biological materials. *Acta Mech. Solida Sin.* 29 (3), 245–256.
- Woo, S.L., Johnson, G.A., Smith, B.A., 1993. Mathematical modeling of ligaments and tendons. *J. Biomech. Eng.* 115 (4B), 468–473.
- Yamaoka, H., Adachi, T., 2010. Coupling between axial stretch and bending/twisting deformation of actin filaments caused by a mismatched centroid from the center axis. *Int. J. Mech. Sci.* 52 (2), 329–333.
- Zhao, Z., Li, B., Feng, X., 2016. Handedness-dependent hyperelasticity of biological soft fibers with multilayered helical structures. *Int. J. Non-Linear Mech.* 81, 19–29.